Desalination and Water Treatment
www.deswater.com
doi: 10.5004/dwt.2019.24636

167 (2019) 13–26
November

An alternative strategy for enhanced algae removal by cationic chitosan-based flocculants

Yongjun Sun[a,*], Jianwen Liu[a], Wenquan Sun[a], Huaili Zheng[b], Kinjal J. Shah[a,*]

[a]*College of Urban Construction, Nanjing Tech University, Nanjing 211800, China, emails: sunyongjun@njtech.edu.cn (Y.J. Sun), d10122801@mail.ntust.edu.tw (K.J. Shah)*
[b]*Key Laboratory of the Three Gorges Reservoir Region's Eco-Environment, State Ministry of Education, Chongqing University, Chongqing 400045, China*

Received 21 February 2019; Accepted 29 June 2019

ABSTRACT

The water solubility and polymerizability of maleoyl chitosan (MCS) was significantly improved by introducing a maleoyl group into the chitosan chain and MCS is a promising monomer for preparing chitosan-based flocculants with good water solubility. In this study, MCS was grafted with acrylamide and diallyldimethylammonium chloride to prepared a cationic chitosan modified flocculant chitosan-graft-poly (acrylamide diallyldimethylammonium chloride) (PMAD) with excellent solubility by ultraviolet (UV)-induced copolymerization techniques. The effects of monomer concentration, the percentage of maleated chitosan, photoinitiator concentration and illumination time on the intrinsic viscosity, grafting efficiency and dissolution time of PMAD were investigated by single factor experiments. The optimal synthesis conditions were determined with monomer concentration 12.5%, MCS percentage 10%, cationicity 11.25%, photoinitiator concentration 0.3% and illumination time 120 min, proving that UV initiated method was benefited to improve water solubility of PMAD. PMAD prepared at the optimized condition has the optimal viscosity of 4,823.2 mg L^{-1}, the grafting efficiency of 70.7% and the dissolution time of 75 min. At the same time, the synthesized products PMAD were characterized by infrared spectroscopy, scanning electron microscopy, H-nuclear magnetic resonance, thermogravimetric and X-ray diffraction techniques. The flocculation experiments of PMAD on algae-containing water showed that the flocculation performance of PMAD was remarkably higher than that of commercially available polyacrylamide and polyaluminum ferric chloride. The optimal removal rate of Chl a (81.2%), turbidity (94.9%), and algae cell concentration (99.7%) by PMAD was obtained at dosage of 40 mg L^{-1}, pH value 8 and *G* value 500 s^{-1}. The obtained zeta potential results proved that the main flocculation mechanism of PMAD was the function of adsorption bridging.

Keywords: Chitosan-based flocculant; Graft copolymerization; Enhanced flocculation; Algae removal; Photopolymerization

1. Introduction

In recent years, the eutrophication caused by increasing nitrogen and phosphorus nutrients in water bodies has caused algae in many lakes and reservoirs which can be resulted to "water blooms". During the growth process, algae cells will aggregate to form algae cell clusters and the organic matter produced by the metabolism of algae cells will be released into the water body. In general, studies showed that algae cells were hydrophilic and negatively charged organism with low specific gravity and [1] good solubility, which is responsible for maintaining the quality of the water [2]. When the blooms broke out, a large number of algae covered the surface of the water, causing a

* Corresponding authors.

sharp drop in dissolved oxygen content in the water, which resulted to large number of aquatic organisms dying and greatly destroying the aquatic ecosystem. At the same time, algae can produce algae toxins that harm organisms, posing a great threat to human health. The outbreak of algae blooms will also affect the water production of water plants. On the one hand, it is difficult to remove a large number of algae cells by conventional coagulation process due to the electrostatic repulsion, surface hydrophilicity and steric hindrance of algae cells [3]. Meanwhile, on the other hand, algae cells, due to their small size, penetrate the filter pool and cause the filter to clog. Based on the adverse effects of algae blooms on aquatic ecosystems and human health, it is a hot topic for researcher to develop effective processes for algae removal and eliminate algae pollution.

Flocculation is a one of the most economical, common and important methods in water treatment, and is indispensable as one of the important operating units for water treatment. The flocculation method removes pollutants and colloidal particles from water with simple treatment process, low cost, high efficiency, large treatment water volume, and wide application range. If the algae in the raw water can be effectively removed by economical and simple flocculation method without increasing the additional process, the water treatment enterprise can save a large cost. Simultaneously, the flocculation method does not destroy the algae cells, there by reducing the release of algae toxins and decreasing disinfection byproducts with higher safety. Conventional inorganic coagulants are often susceptible to coexisting ions and the algae cell particles are fine with the slow floc formation speed and small floc particle size during the coagulation process coagulated by inorganic coagulants. In addition, the floc density is small with weak strength, leading to poor sedimentation performance and low removal efficiency in the conventional coagulation process. Therefore, how to synthesize green and high-efficient flocculant to form compact flocs which are easy to be settled during flocculation is an urgent problem to be solved at present, which is of great significance for solving the problem of algae removal in the water supply. Due to the high negative charge of algae in the water, conventional dosages of coagulants are difficult to neutralize electrically to achieve effective coagulation. Therefore, it is necessary to increase the dosage of the flocculants to achieve the purpose of charge neutralization. In addition, the removal efficiency of $FeCl_3$ and polymeric iron salts is low at same dosage compared to organic flocculants, which may cause changes in the chromaticity of the supernatant with large sludge production after coagulation, leading to high sludge subsequent treatment costs [4]. Moreover, the extracellular substances secreted by the algae cells can undergo an integration reaction or a complexation reaction with the coagulant cations, thereby hindering the coagulation process of the algae. Therefore, the research and development of new flocculants with high efficiency in algae removal and low cost has become an urgent problem to be solved in current water treatment and is of great significance for ensuring the safety of drinking water.

In recent years, chitosan has received widespread attention as a natural organic polymer flocculant which is nontoxic and harmless and has a wide range of sources [5]. Chitosan is a natural basic aminoglycan substance; its flexible linear molecular chain structure of chitosan makes it play a role of "Adsorption Bridge" with many extremely active and adjacent hydroxyl and amino groups distributed on the molecule [6]. The amino group in the molecular chain is protonated in aqueous solution, which is well-adsorbed with the negatively charged algae cells with good flocculation performance [7]. However, a large number of studies have shown that due to the poor solubility of chitosan, it is only soluble in weak acidic solutions with low molecular weight, which limits its application as a flocculant [8]. To overcome these shortcomings, the researchers adopt several modification methods to modify chitosan to obtain highly efficient chitosan-based flocculants [9], such as quaternization [10], acylation [11], carboxylation [12], etherification [13], graft modification [14] and other modification methods for introducing chemically functional groups to improve the physical and chemical properties of chitosan [15]. In addition, chitosan molecules with many reactive groups are prone to graft copolymerization. Graft copolymerization modification can not only increase the molecular weight of chitosan-based flocculant, but also increase the adsorption site on the chitosan chain, so it can significantly improve its flocculation capacity.

The ultraviolet (UV) initiation method is characterized by easy control, rapid initiation and pollution free, and the synthesized polymer with high purity, good linearity and good solubility can be obtained. In order to prepare a multifunctional green flocculant with high removal efficiency of algae removal, UV light initiation is employed in this study. In this research, malely chitosan is prepared based on our previously reported work, and chitosan-graft-poly (acrylamide diallyldimethylammonium chloride) (PMAD) flocculant was prepared by using maleoyl chitosan (MCS), acrylamide (AM), and diallyldimethylammonium chloride (DMDAAC) as comonomers through UV-induced grafting polymerization [16]. The effects of monomer concentration, monomer ratio, photoinitiator concentration and initiation time on the intrinsic viscosity, grafting efficiency and dissolution time of PMAD were investigated. The microstructure of PMAD was characterized by scanning electron microscopy (SEM), Fourier transforms infrared spectroscopy (FTIR) and infrared spectroscopy (X-ray diffraction (XRD)). PMAD was used to flocculate the algae-containing water for determining its flocculation capacity, and flocculation results in comparisons with polyacrylamide (PAM) and polyaluminum ferric chloride (PAFC) were explored. The mechanism of the flocculation process for removing algae was also discussed by zeta potential results.

2. Materials and methods

2.1. Materials

Chitosan (CS), 2,2-azobis (2-methylpropionamidine) dihydrochloride (V50) and diallyldimethylammonium chloride solution (DMDAAC, 60% by weight in water) were purchased from Shanghai Aladdin Biochemical Technology Co. Ltd., China. AM and sodium chloride (NaCl) were obtained from SinopHarm Chemical Reagent Co. Ltd., China Maleic. anhydride (MAH) was obtained from SinopHarm Chemical Reagent Co. Ltd., China High-purity nitrogen (N_2) was

purchased from Nanjing Sale Electronic Information Industry Group Co. Ltd., China. In addition, acetone and ethanol were purchased from Shanghai Zhenqin Chemical Reagent Co. Ltd., China. PAM and PAFC were sourced from Nanjing Shengjianquan Glass Instrument Co. Ltd., China. All reagents used in this study were of analytical grade and used without any further purification.

2.2. Preparation of PMAD

MCS was prepared using a method with MAH and CS, which has been reported in our previously published works [16]. 7.640g CS was dissolved in 100 mL of 2% (wt.) acetic acid and 4.589g MAH was dissolved in 10 ml H_2O, they were mixed together with magnetic stirrer after dissolved. Then, this mixture was placed in a water bath with 30°C for 7 h to prepare MCS. A certain amount of MCS was dissolved in water and then mixed with AM and DMDAAC [17]. Thereafter, the mixture was grafted with UV radiation in a 125 mL quartz vessel after filled with nitrogen for 5 min and added with a certain amount of 2,2-azobis (2-methylpropionamidine) dihydrochloride (V50) used as the photoinitiator. The sample was matured for 1 h. Finally, the obtained sample solution was purified by a mixed solution of acetone and ethanol in a volume ratio of 2:1 and then dried in an oven at 105°C for 24 h until a constant weight was obtained. The dried product was ground and sieved through a 100 mesh sieve to obtain the final product. A schematic diagram of PMAD synthesis is shown in Fig. 1.

2.3. Characterization

In order to explore the structure of PMAD, several samples were characterized, including: CS, P(AM-DMDAAC), PMAD whose monomer ratio is mMCS:mAM:mDMDAAC = 1:5:4 (hereinafter referred to as PMAD1), PMAD whose monomer ratio is mMCS:mAM:mDMDAAC = 1:6:3 (hereinafter referred to as PMAD2). The electron microscopy powder and the purified products were adhered to the conductive adhesive and were placed in a SEM (JSM-5900, JEOL, Japan) after being sprayed with gold to observe changes in surface morphology; The obtained final products were analyzed by an X-ray diffractometer (ARL X'TRA, Thermo Electron Corporation, USA) to obtain the diffraction patterns. The products were placed in a FTIR spectrometer (Nexus 670, Electron Corporation, USA) to perform an analysis to obtain an infrared spectrum. The products were analyzed by a nuclear magnetic resonance (NMR) spectrometer (BRUKER Company, Switzerland) to obtain a NMR spectrum. The purified and dried product was placed in a differential thermal analyzer (SHIMADZU, Japan) to obtain a thermogravimetric analysis chart. The intrinsic viscosity, graft efficiency and dissolve time of PMAD were measured according to technical specification and test method of water treatment chemical cationic PAMs (GB/T 31246-2014).

2.4. Flocculation tests for algae removal

The algae-containing wastewater was placed in a 500 ml beaker and subjected to a flocculation test using a coagulation mixer. The initial pH of the wastewater was adjusted by 0.1 mol L^{-1} dilute hydrochloric acid (HCl) or sodium hydroxide (NaOH) aqueous solution. After a certain amount of flocculant was added to the water sample, the mixture was vigorously stirred at a certain speed gradient (G^{-1}) 350 r min^{-1} of for 3 min, then stirred at 70 rpm for 15 min, and finally allowed to stand for 15 min. After flocculation, the supernatant was separated to determine residual turbidity, chlorophyll a (Chl-a), algae cell density removal rate and zeta potential. Among them, the content of Chl-a is determined by referring to "Determination of chlorophyll (spectrophotometric method)" (SL 88-2012 [18]). Algae cell concentration was determined according to the "Chemicals-Alga growth inhibition test" (GB/T 21805-2008 [19]). The Zeta potential was measured by a zeta potential analyzer (Malvern Zetasizer Nano ZS90, Malvern Instruments Ltd., England) with reference to "Colloidal System-Methods for Zeta Potential Determination" (GB/T 32671.1-2016 [20]).

$$\text{Chl}-\text{a removal efficiency}(\%) = \frac{\rho_{\text{chl}-\text{a}}(\text{before}) - \rho_{\text{chl-a}}(\text{after})}{\rho_{\text{chl-a}}(\text{before})} \times 100\% \quad (1)$$

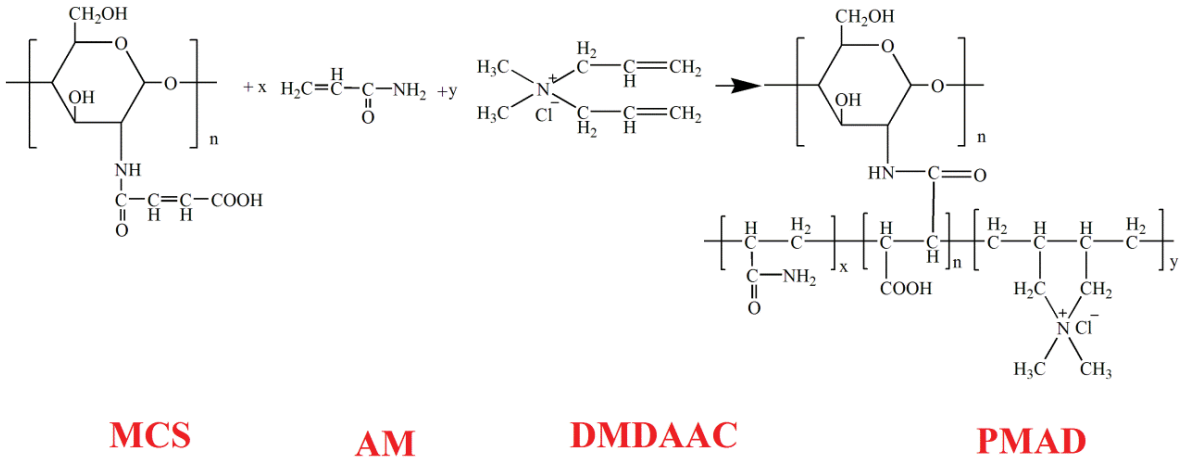

Fig. 1. Schematic diagram of PMAD synthesis.

where $\rho_{chl\text{-}a}$ (before) is the concentration of Chl-a before flocculation in μg L^{-1}; and $\rho_{chl\text{-}a}$ (after) is the concentration of Chl-a after flocculation in μg L^{-1}.

$$\text{Turbidity removal efficiency}(\%) = \frac{\text{turbidity}(\text{before}) - \text{turbidity}(\text{after})}{\text{turbidity}(\text{before})} \times 100\% \quad (2)$$

where turbidity (before) is the turbidity value before flocculation in NTU and turbidity (after) is the turbidity value after flocculation in NTU.

$$\text{Algal cell removal efficiency}(\%) = \frac{\text{Algal cell}(\text{before}) - \text{Algal cell}(\text{after})}{\text{Algal cell}(\text{before})} \times 100\% \quad (3)$$

where algal cell (before) is the algal cell number value before flocculation and algal cell (after) is the algal cell number value after flocculation.

3. Results and discussion

3.1. Optimization of synthetic condition

3.1.1. Effect of monomer concentration

As shown in Fig. 2, the intrinsic viscosity of PMAD tended to increased and then decreased as the monomer concentration increased. The intrinsic viscosity reached a maximum value of 4,823.2 mL g with a monomer concentration of 12.5%. The graft efficiency decreased and then increased with monomer content, and its value was basically stable at 91.5% when the monomer concentration was over 22.5%. The dissolution time increased with monomer concentration. Especially, as the concentration increased from 20% to 22.5%, the PMAD dissolution increased sharply from 71 to 120 min.

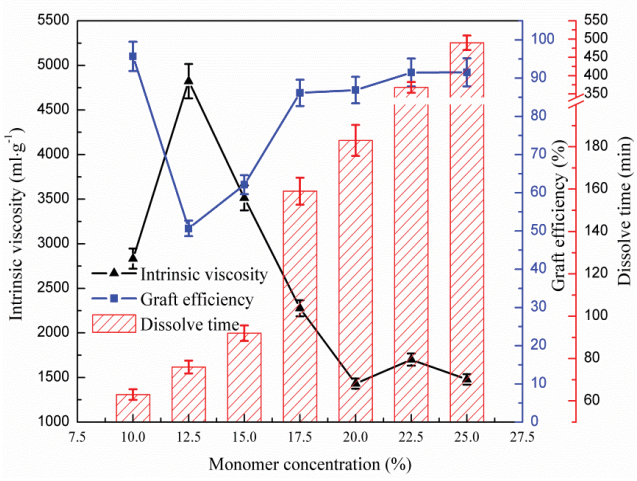

Fig. 2. Effects of monomer concentration on intrinsic viscosity, graft efficiency and dissolve time.

These results may be attributed to the following reasons: at low monomer concentration, the primary radical was hard to be collided with the monomer and resulting in a low reactivity [17]. So, it was difficult to form the macromolecular graft copolymer, leading to low intrinsic viscosity. As the monomer concentration increased, the primary radical reacts with the monomer to form a large amount of active monomer, promoting the reaction speed of the chain propagation. Hence, a long-chain structure of the polymer was formed with the increasing the intrinsic viscosity. With the continues increment of monomer concentration, the collision between the primary radical and the monomer was saturated, so the macromolecular chain will not continue to grow [21]. Moreover, since the monomer concentration was saturated, the active free radicals easily interact with each other, leading to the inactivation of them [22]. This may also cause a chain transfer reaction, resulted to the transfer of chain radicals to the monomer, and thus the intrinsic viscosity decreased. As the monomer concentration increased, the probability of collision between free radicals increased, increasing graft efficiency. When the monomer concentration was not saturated, the chain propagation was promoted with the monomer concentration. At the same time, the chain structure produced by the grafting reaction is long with a high molecular weight [23], and the dissolution time also increased. However, when the monomer concentration was saturated, the crosslinking reaction occurs between some monomer molecules, resulting in poor solubility and increasing dissolution time.

3.1.2. Effect of DMDAAC proportion

The further study was conducted with MCS content of 10% and 20% in consideration of the PMAD dissolution time. As shown in Fig. 3, the intrinsic viscosity of PMAD increased first then decreased while graft efficiency and dissolution time decreased continuously with the increase of DMDAAC content. The intrinsic viscosity and graft efficiency of PMAD with 20% MCS content was higher than that with 10% MCS content, but the dissolution time of PMAD with 10% MCS content is higher than that with 20% MCS content. When the content of DMDAAC was 10%, the graft efficiency is the highest. When the content of DMDAAC reached 40%, the intrinsic viscosity of PMAD reached the maximum of 6420.3 mg L^{-1} with 40% DMDAAC and 10% MCS content, and the dissolution time was basically stable.

This is because the relative content of AM monomer decreasing with the content of DMDAAC, resulting in a decrease of probability in AM grafting onto the MCS chain [24]. So the active sites on the MCS chain cannot be effectively utilized and the graft efficiency decreased continuously. When the content of DMDAAC increased from 10% to 40%, the content of DMDAAC monomer and AM monomer was getting closer. When the DMDAAC content reaches 40%, the probability of grafting AM and DMDAAC onto the MCS chain was equivalent. At this time, the PMAD structure was relatively complete, so the intrinsic viscosity was large [22]. The dissolution time of PMAD with 20% MCS content was significantly greater than that with 10% MCS content. The intrinsic viscosity and graft efficiency of PMAD with MCS content of 10% were significantly greater than that of 20%.

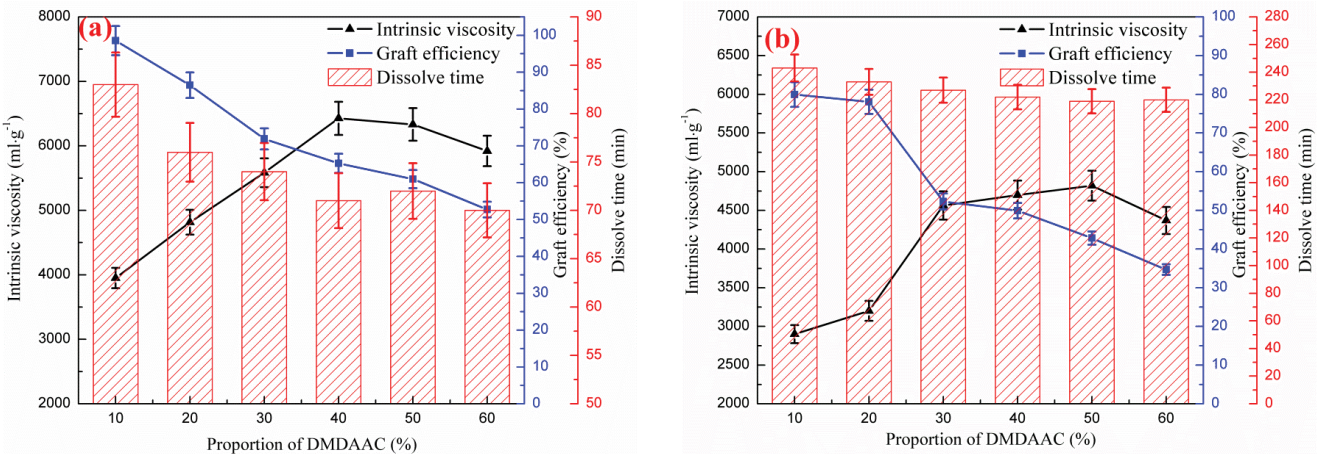

Fig. 3. Effects of proportion of DMDAAC with (a) 10% MCS and (b) 20% MCS on intrinsic viscosity, graft efficiency and dissolve time.

It was due to the content of MCS was more than 10%, excessive MCS reduces the content of AM and DMDAAC. Hence, AM and DMDAAC free radicals were less in the mixture and slow down the chain reaction rate [25]. The probability of diffusion grafting onto the MCS chain was also relatively low. Therefore, the intrinsic viscosity and graft efficiency of PMAD were lower.

3.1.3. Effect of photoinitiator concentration

As shown Fig. 4, when the photoinitiator content increased from 0.1% to 0.6%, the intrinsic viscosity and graft efficiency rose sharply, decreased slowly. When the amount of the photoinitiator was 0.3%, the intrinsic viscosity and the graft efficiency reached a maximum value, at which the intrinsic viscosity was 4,823.2 mg L^{-1} and the graft efficiency was 70.7%. As the photoinitiator content increased, the dissolution time increased continuously. When the photoinitiator content was 0.6%, the dissolution time reached a maximum value of 85 min.

This is because that, very few primary free radicals are existent to react with the monomers at low initiator content. At the same time, the primary radicals decomposed by initiator molecules were always surrounded by a high viscosity polymer solution. The solution contains a large amount of solvent molecules. Part of the free radicals cannot be contacted with monomer molecules, so the initiation efficiency and the chain reaction rate were lower, resulting in a "cage effect" and leading to a low value of intrinsic viscosity, graft efficiency and dissolution time. The heat generated by the decomposition of the initiator molecules and the chain reaction rate increased with the initiator content. And the free radicals continuously react to form a macromolecular structure, resulted in the increase of the intrinsic viscosity, graft efficiency and dissolution time. When the content of the initiator was too large, the excess initiator makes the heat of the solvent increase rapidly for a short time [26], leading to a great increase in the chance of cross-linking and implosion and the decrease of the intrinsic viscosity and graft efficiency. Therefore, in the present study, the synthesis condition was optimized with the photoinitiator content of 0.3%.

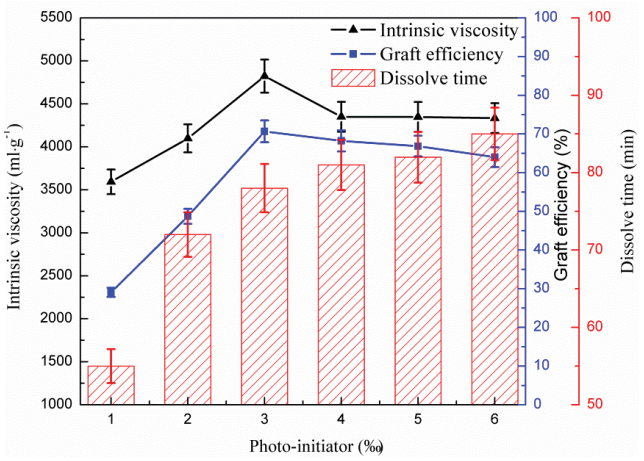

Fig. 4. Effects of photo-initiator dosage on intrinsic viscosity, graft efficiency and dissolve time (monomer concentration: 12.5%, mMSC:mAM:mDMDAAC = 1:5:4, radiation time: 2 h.).

3.1.4. Effect of photochemical reaction time

As shown in Fig. 5, the dissolution time, graft efficiency and intrinsic viscosity increased first then slowly decreased with the increasing of dissolution time. The intrinsic viscosity, dissolution time and graft efficiency reached to a maximum of 4,823.2 mg L^{-1}, 70 min, 70.7% at radiation time 2 h, respectively. When the dissolution time was short, very little energy can be generated by the UV light irradiation. So the initiator was difficult to be decomposed into free radicals. Therefore, the probability of free radicals colliding with each other is small and the chain reaction rate is slow. The intrinsic viscosity, graft efficiency and dissolution time were all low at this time. As the illumination time increased, the energy generated by UV light irradiation became larger. The photoinitiator fully reacted to decompose and form a large amount of primary radicals. It promotes chain propagation and forms macromolecular chains rapidly. So graft efficiency, intrinsic viscosity and dissolution time became larger. When the illumination time was too large, the photoinitiator had been completely decomposed into primary

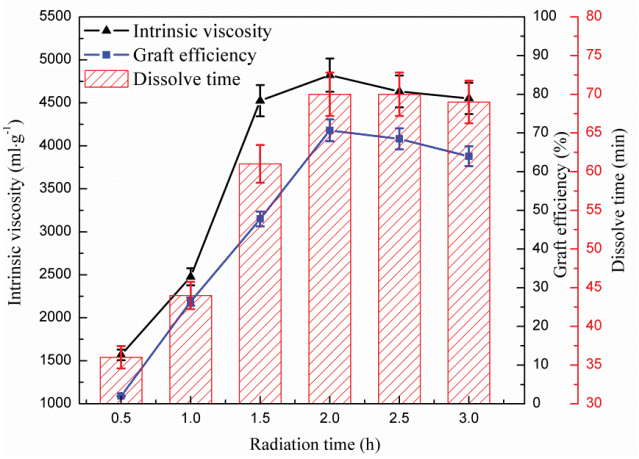

Fig. 5. Effects of radiation time on intrinsic viscosity, graft efficiency and dissolve time (monomer concentration: 12.5%, mMSC: mAM:mDMDAAC = 1:5:4, photo-initiator concentration: 3‰.).

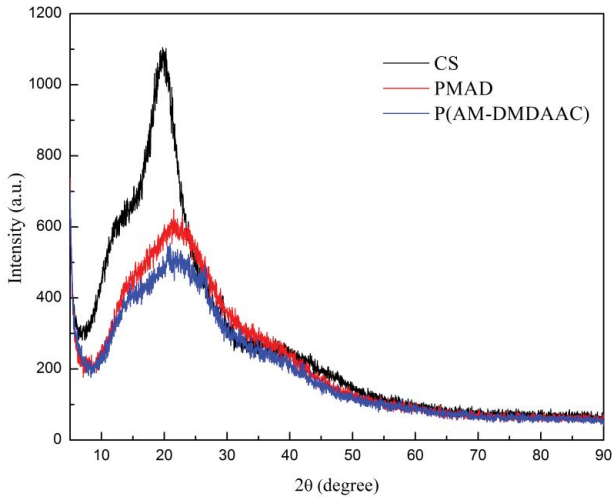

Fig. 6. XRD spectrum of CS, P(AM-DMDAAC), PMAD.

radicals. The amount of primary radicals has reached a supersaturation state, colliding with the previously formed macromolecular chains, destroying the structure of some molecular chains, and increasing the possibility of chain transfer and chain termination reaction.

3.2. Morphological and structural characterization of PMAD

3.2.1. XRD spectrum results

XRD of CS, P(AM-DMDAAC) and PMAD was carried out to investigate the structural change of the polymer PMAD during graft polymerization. As shown in Fig. 6, CS exhibits a narrow and steep diffraction peak at 2θ = 20°, it corresponds to the crystal structure in CS. when 2θ is 22°, P(AM-DMDAAC) has a broad and gentle diffraction peak at 2θ = 22°. PMAD showed a broad and gentle diffraction peak at 2θ = 22°. The diffraction values of P(AM-DMDAAC) and PMAD at the diffraction peak 2θ = 22° are lower than that of CS.

There are hydroxyl groups and amino groups distributing on the CS molecular chain, which formed intramolecular and intermolecular hydrogen bonds. Furthermore, due to the existence of hydrogen bonds and the regularity of molecules, CS tends to form tiny crystal structures locally. With the introduction of AM and DMDAAC, the hydrogen bond of the CS molecule will be broken. So the order of the formed crystal structure was destroyed, and the overall structural order of the polymer PMAD is greatly reduced. The peak value of PMAD is smaller than that of P(AM-DMDAAC), which indicates that the structural order of PMAD is destroyed more completely than that of P(AM-DMDAAC), indicating that the solubility of PMAD was better than that of P(AM-DMDAAC). The research also illustrates indirectly the success of photoinitiated graft polymerization of AM, DMC, and MCS simultaneously.

3.2.2. SEM analysis

In ordered to observe the surface morphology of the copolymer, CS, P(AM-DMDAAC) and PMAD were magnified 1,000×, 3,000× and 5,000× respectively. The crystal structure was observed and analyzed. As shown in Fig. 7a, the surface of the CS is flat and smooth. And the surface has no obvious holes, which was in the form of a sheet. As shown in Fig. 7b, the surface of P(AM-DMDAAC) was smooth and has a few holes, it is in the form of a block. As shown in Fig. 7c, the surface of the PMAD became rough. Meanwhile, the layered structure was destroyed. There is a pore-like structure whose pores are tiny. The bulk and layered structures are destroyed because of the grafting of AM and DMDAAC. This irregular pore structure increased the specific surface area of the copolymer [27].

3.2.3. FTIR spectra

As shown in the infrared spectrum of PMAD (Fig. 8), the stretching stress peaks at 3,419 and 3,177 cm^{-1} were caused by the hydroxyl group (–OH) and amino-group ($–NH_2$) in the MCS unit and the $–NH_2$ group in the AM unit [28]. The absorption peak at 2,936 cm^{-1} was attributed to the stretching vibrations of carbon-hydrogen bond (C–H), it was caused by methylene ($–CH_2–$) and methyl group (–CH3) in the DMDAAC unit and the hydroxymethyl group ($–CH_2OH$) in the CS unit. The absorption peak at 1,652 cm^{-1} was attributed to the carbonyl (C=O) stretching vibration peak and was caused by the amide group ($–CONH_2$) of the MCS unit and the AM unit [29]. The absorption peak at 1,309 and 1,405 cm^{-1} resulted from the carbon-nitrogen (C–N) bond, it was caused by the –NHCOCHCHCOOH in the MCS unite and $–CONH_2$ in the AM unite [30].

Compared with the C–H stretching vibration peak of CS at 2,894cm^{-1}, the C–H stretching vibration peak of PMAD appears blue shift; this is because the substituent replaces the hydrogen on the CS molecular chain in the polymerization reaction. carbonyl group (C=O) stretching vibration peak appeared on the infrared spectrum of PMAD but C=C vibration peak did not appear. This indicates that C=C in the MCS and DMDAAC molecules was opened, and an addition reaction occurs, indicated that AM and DMDAAC monomers were successfully grafted to the chitosan chain. The characteristic absorption peaks of P(AM-DMDAAC)

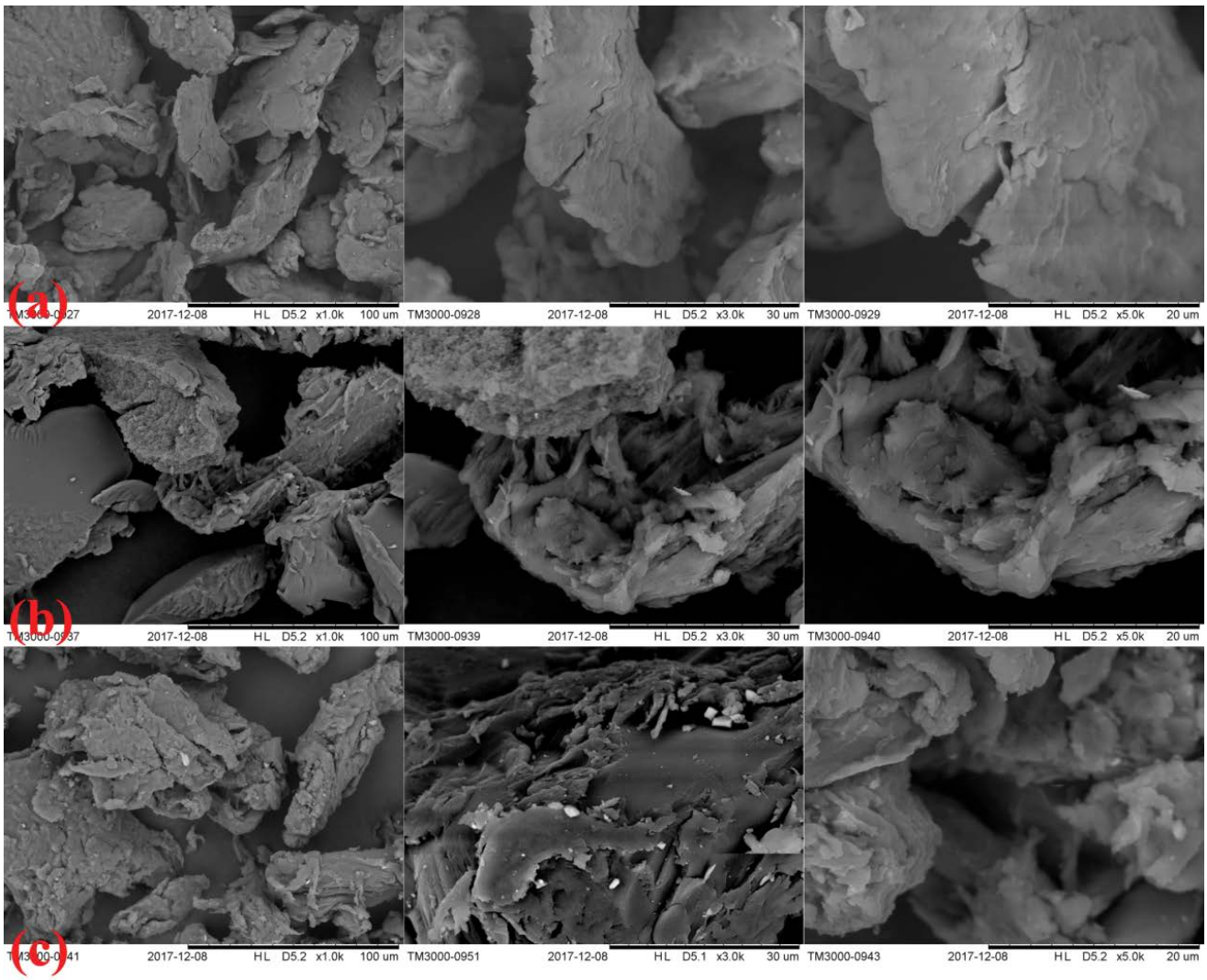

Fig. 7. SEM images of CS, P(AM-DMDAAC) and PMAD: (a) CS, (b) P(AM-DMDAAC) and (c) PMAD.

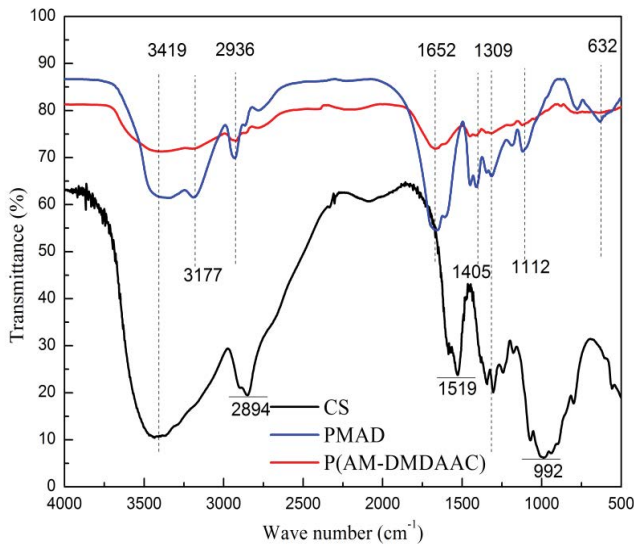

Fig. 8. FTIR spectra of CS, P(AM-DMDAAC) and PMAD.

and CS were shown in the infrared spectrum of PMAD, and some characteristic absorption peaks and vibration absorption peaks were blue-shifted, indicating that MCS, AM, and DMDAAC were successfully graft copolymerized.

3.2.4. Thermogravimetry-differential thermal analysis (TG-DTC) characterization

The results in Fig. 9 show that the pyrolysis process of CS includes three stages in the range of 20°C–800°C. The weight loss temperature ranged of the first stage is 20°C–200°C. The weight loss rate of CS was 5.67%, and the maximum weight loss temperature was 62.13°C in this range. It is caused by the loss of the adsorbed water and the bound water in the sample [31]. The weight loss temperature range of the second stage was 200°C–800°C. The weight loss rate of CS was 55.76%, and the maximum weight loss temperature was 295.18°C. The reason for weight loss may be that the polymerization degree of CS is affected by high temperature, which leads to the decomposition of CS. In the final stage, the decomposition temperature was about 800°C,

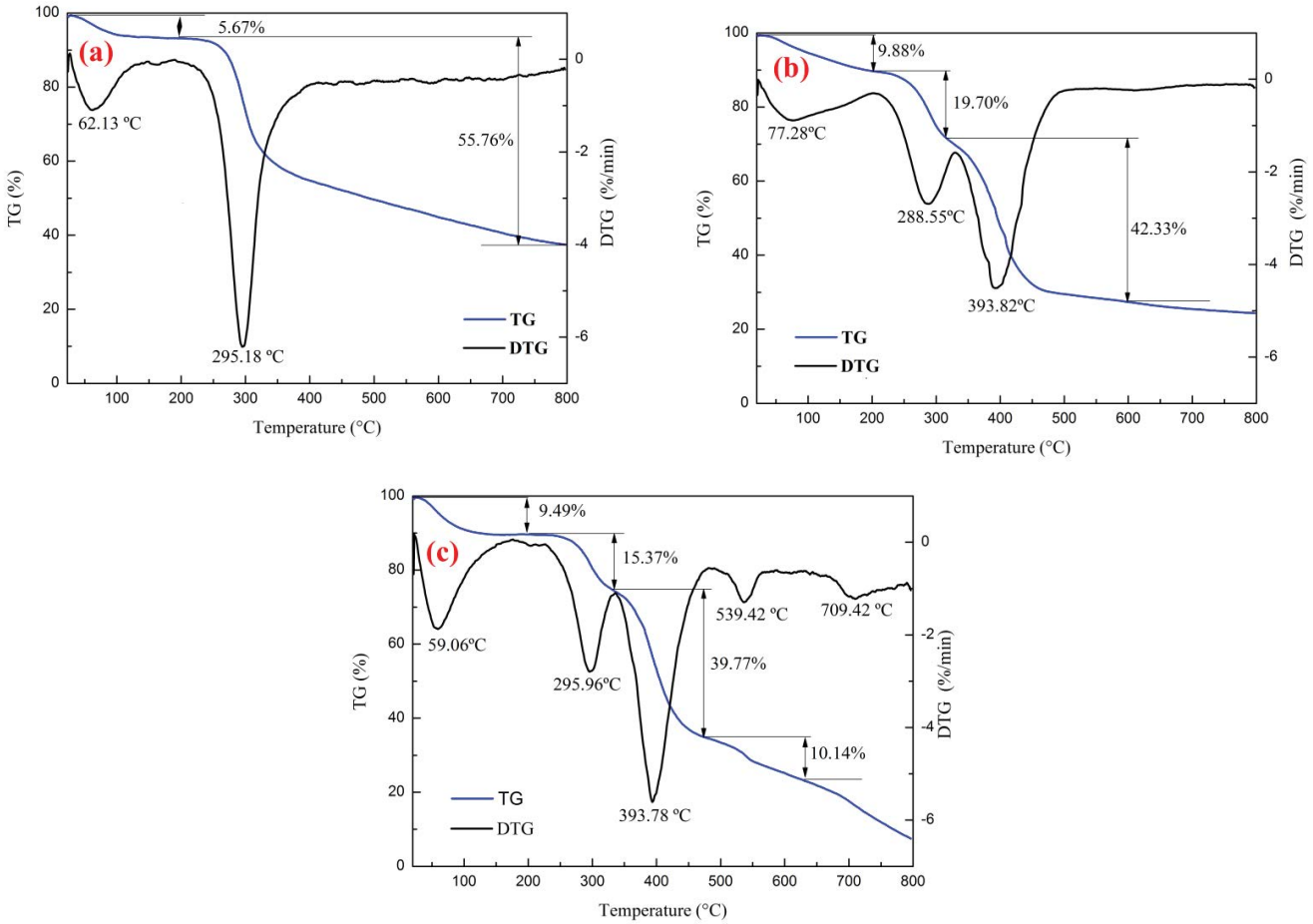

Fig. 9. TG-DTG curve of CS, P(AM-DMDAAC) and PMAD: (a) CS, (b) P(AM-DMDAAC) and (c) PMAD.

after which the thermogravimetric curve tends to be stable without weight loss. The final residual amount was about 37.46%. As shown in Fig. 9b, P(AM-DMDAAC) has three stages of weight loss in the range of 20°C–800°C. The weight loss temperature range of the first stage was 20°C–200°C. The weight loss rate of the sample was 9.88%, and the maximum weight loss temperature was 77.28°C in this range. This is caused by the dehydration of the sample. The weight loss temperature ranged of the second stage was 200°C–300°C. The weight loss rate of the sample was 19.70%, and the maximum weight loss temperature was 288.55°C in this range. The reason might be that the $–CONH_2$ of the AM unit was thermally decomposed [32]. The weight loss temperature ranged of the third stage was 300°C–600°C. The weight loss rate of the sample was 42.33%, and the maximum weight loss temperature was 393.82°C in this range. After 600°C, the thermogravimetric curve tended to be stable without weight loss, and the final residual weight is 24.33%. It can be seen from Fig. 9c that PMAD has four stages of weight loss in the range of 20°C–80°C. The weight loss temperature ranged of the first stage was 20°C–180°C, the weight loss rate of the sample was 9.49%, and the maximum weight loss temperature was 59.06°C in this range. The weight loss at this stage is due to the removal of adsorbed water and crystal water. In the second stage, the weight loss range was 180°C–320°C, the weight loss of the sample was 15.37%, and the maximum weight loss temperature was 295.92°C. The weight loss may be caused by thermal decomposition of the amide group; the weight loss range of the third stage is 320°C–480°C. In this range, the sample weight loss was 39.77%, the maximum weight loss temperature was 539.42°C, the weight loss may be caused by the five-membered ring introduced by the DMDAAC unit [33]; the fourth stage weight loss range was 480°C–630°C, the sample weight loss in this range 10.14%, the maximum weight loss temperature was 709.42°C, the final decomposition temperature is about 630°C and the final residual weight was 23.13%.

The thermal decomposition temperature of CS, P(AM-DMDAAC) and PMAD were 295.18°C, 393.82°C and 709.42°C, respectively. The thermal decomposition temperature of PMAD was significantly larger than that of CS and P(AM-DMDAAC), demonstrating that the thermal stability of PMAD is remarkably improved after grafting.

3.2.5. ^{1}H-NMR Analysis

As shown in Fig. 10a, the resonance peaks of PMAD at 6.15 and 5.86 ppm were attributed to the amino hydro proton peak of $–CONH_2$ in the AM unit [34]; the resonance peak at 4.02 ppm corresponds to the methylene group of $–CH_2Cl$ in

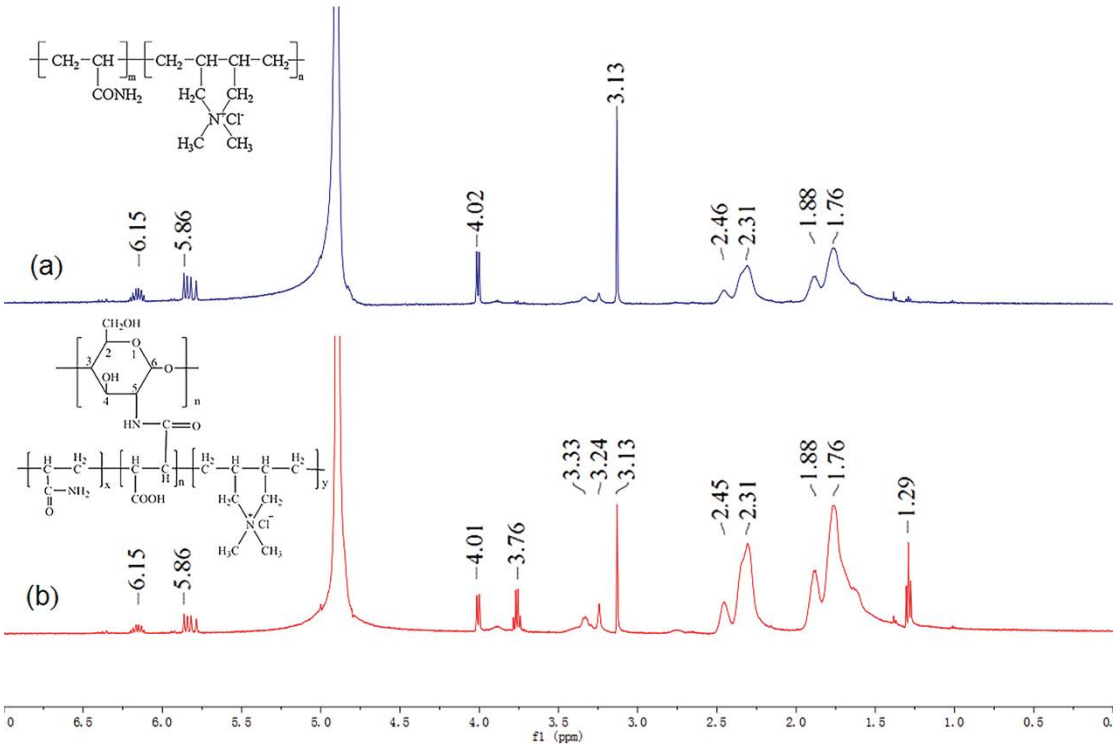

Fig. 10. ^{1}H-NMR spectrum of P(AM-DMDAAC) and PMAD: (a) P(AM-DMDAAC) and (b) PMAD.

the AM unit and the proton peak of –OH hydrogen on the ring of the MCS unit. The resonance peak at 3.76 ppm was caused by the methylene hydrogen (–CH_2–) of –CH_2OH on the MCS unit ring. The absorption peak at 3.33 ppm was assigned to the protons for –N(CH_3) in DMDAAC unit. And the resonance peak at 3.13 ppm was caused by the methylene hydrogen (–CH_2–) of –CH_2OH on the MCS unit ring. [35]. The resonance peak at 2.45 and 2.31 ppm corresponds to the proton peak of the –COCH– in the AM group [36]. The characteristic peaks at 1.88, 1.76 and 1.29 ppm correspond to the –CH–, which is caused by the amide group after opening double bond in the MCS unit, the –CH_2–CH–$CONH_2$ in the AM unit and the five-membered ring in the DMDAAC unit, respectively [37].

Comparing Figs. 10a and b, it can be found that the characteristic peaks of PMAD include all the characteristic peaks in MCS unit, AM unit and the DMDAAC unit, indicating that the MCS, AM and DMDAAC monomers have successfully polymerized.

3.3. Flocculation performance

3.3.1. Effect of dosage on flocculation effect

As shown in Fig. 11, the removal rate of turbidity increased with the dosage and then decreased slowly. When the dosage of PMAD and PAM reached 6 mg L^{-1} and PAFC reached 40 mg L^{-1}, the turbidity removal efficiency was optimal. At this condition, the removal rate of turbidity by PMAD, PAM and PAFC are 75.7%, 70.2% and 71.5%, respectively. The removal rate of Chl-a increased with dosage but this value decreased with the dosage continue to increased. When the dosage of PMAD and PAM reaches 6 mg L^{-1} and PAFC reaches 40 mg L^{-1}, the Chl-a removal efficiency was optimal. At this time, the removal rate of Chl-a by PMAD, PAM, and PAFC were 70.1%, 61.3% and 65.9%, respectively. At this time, the removal rates of algae cells by PMAD, PAM, PAFC were 76.9 %, 66.7 % and 60%, respectively.

With the increase of dosage, the removal rate of turbidity, Chl-a, and algae cells increased first and then decreased. The flocculant is neutralized with the different negatively charged particles in the water after it is added to the water to form macromolecular particles, which is favorable for sedimentation. When the flocculant dosage was insufficient, the positive charges of the flocculant are unable to neutralize all the colloidal particles [38]. So the turbidity removal rate was low. As the dosage increased, more charges are neutralized which was beneficial for increasing the removal rate. However, when the dosage is too much, the colloidal particles are encapsulated by the flocculant molecules. The negatively charged colloidal particles surface was transferred to a positive charge and reaching the supercharge state. Electrostatic repulsion was re-formed between particles, making the colloidal system stable again [39]. On the other hand, excessive flocculant also forms a certain extent of turbidity. When the dosage content was the same, the flocculation performance of PMAD is significantly better than that of PAM and PAFC. This was due to functional groups such as active amino groups and hydroxyl groups on the molecular chain of the flocculant [40]. What's more,

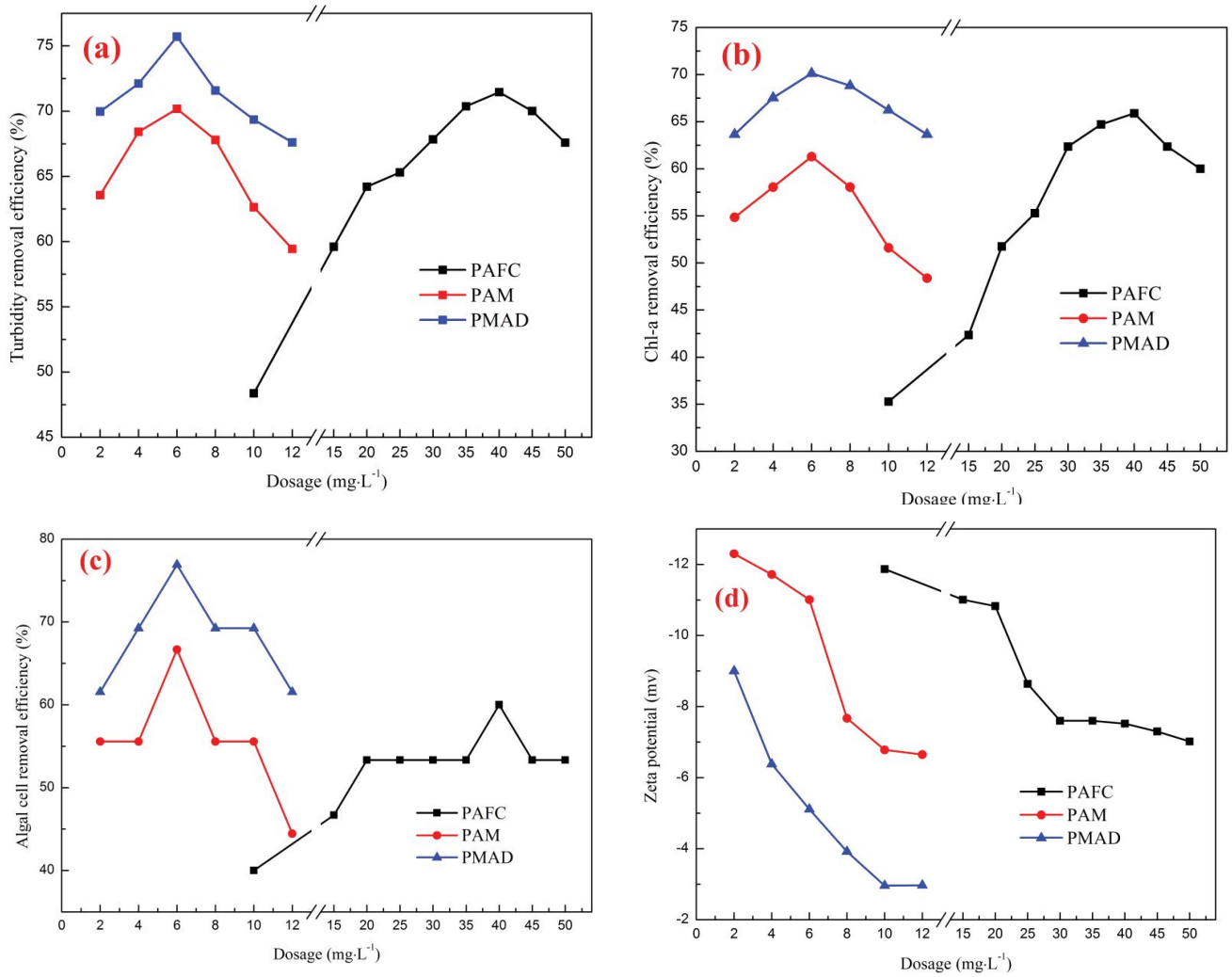

Fig. 11. Effects of dosage on flocculation efficiency: (a) effects of dosage on turbidity removal efficiency, (b) effects of dosage on Chl-a removal efficiency, (c) effects of dosage on algal cell removal efficiency and (d) effects of dosage on zeta potential. (pH: 7, 350 r min^{-1} for 3 min, 70 r min^{-1} for 15 min, sedimentation: 15 min, temperature: 25°C).

the mutual repulsive action of the positive charge in the flocculant allows the main chain to extend to the maximum extent [41]. As shown in Fig. 12, this enhances the adsorption bridging ability and adsorbs different small molecular particles to form larger particles, promoting its destabilization and aggregation [42].

As shown in Fig. 11, when the dosage of PMAD and PAM reached to 10 mg L^{-1} and the PAFC reaches to 30 mg L^{-1}, the zeta potential of the water sample was nearly 0 where optimal flocculation performance obtained simultaneously, indicating that the main flocculation mechanism was charge neutralization. When the dosage of PMAD and PAM was less than 10 mg L^{-1}, the zeta potential was close to zero and no more increase with the dosage. When the dosage of PAFC was less than 30 mg L^{-1}, the zeta potential was close to zero value continuously with the increase of dosage. After reaching 30 mg L^{-1}, the potential tends to be stable. It can be clearly seen from Fig. 11 that when PMAD and PAM with same dosages are added, the zeta potential of the sample water added with PMAD is significantly closer to the value

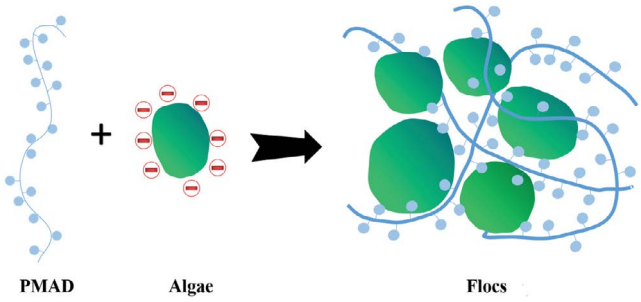

Fig. 12. Schematic diagram of bridging adsorption for algae removal.

of 0 than the potential of the sample water added with PAM [43]. This also showed that the self-made PMAD has better electrical neutralization capacity than the commercially available PAM flocculant. By investigating the effect of dosage on the removal rate of the turbidity, Chl-a and algae

cells, the optimal dosage of PMAD is 6 mg L^{-1}. After careful calculation, the cost of PMAD in the current laboratory conditions is 10–20 RMB Kg^{-1}, while the commercially available PAM is 15–40 RMB Kg^{-1}. The cost price of our prepared cationic organic flocculant PMAD is significantly lower than that of commercially available PAM. The price of PAFC is 1–3 RMB Kg^{-1}, but the dosage of PMAD is only one-tenth of the dosage of PAFC. Compared with the cost of treating unit volume of water, PMAD still has lower cost than that of PAFC.

3.3.2. Effect of pH on flocculation effect

The optimal dosage mentioned in 3.2.1 was used to explore the flocculation performance under different conditions. As shown in Fig. 13, the removal rate of turbidity reaches maxima with a pH of 8. At this pH, the removal rate of turbidity by PMAD, PAM, and PAFC were 87.5%, 75.7% and 71.5%, respectively. The removal rate of turbidity increases with pH and decreased slowly after reaching the maximum value. The removal rate of Chl-a increased with the increasing of pH and decreasing slowly after reaching the maximum value. The removal rate of Chl-a by PMAD, PAM, PFAC at pH 8 was 70.1%, 61.3% and 65.9%, respectively. When the pH was 6, the removal rate of algae cells using PMAD reached 77.8%. When the pH was within 6 to 10, the removal rate of algae cell concentration is constant, indicating that the self-made PMAD has a wide pH range. When the pH was 8, PAFC and PAM have the optimal removal efficiency on algae cell concentration. At this time, the removal rate of algae cell concentration by PAM is 66.77%, and the removal rate of algae cell concentration by PAFC was 60%. The removal rate of algae cell concentration increases with increasing pH and decreases slowly after reaching the maximum value. When the pH was equal, the flocculation performance of PMAD is significantly better than that of PAM and PAFC. While the effect of pH on PMAD is relatively small, indicating that PMAD can be applied to a wide range of pH. As shown in

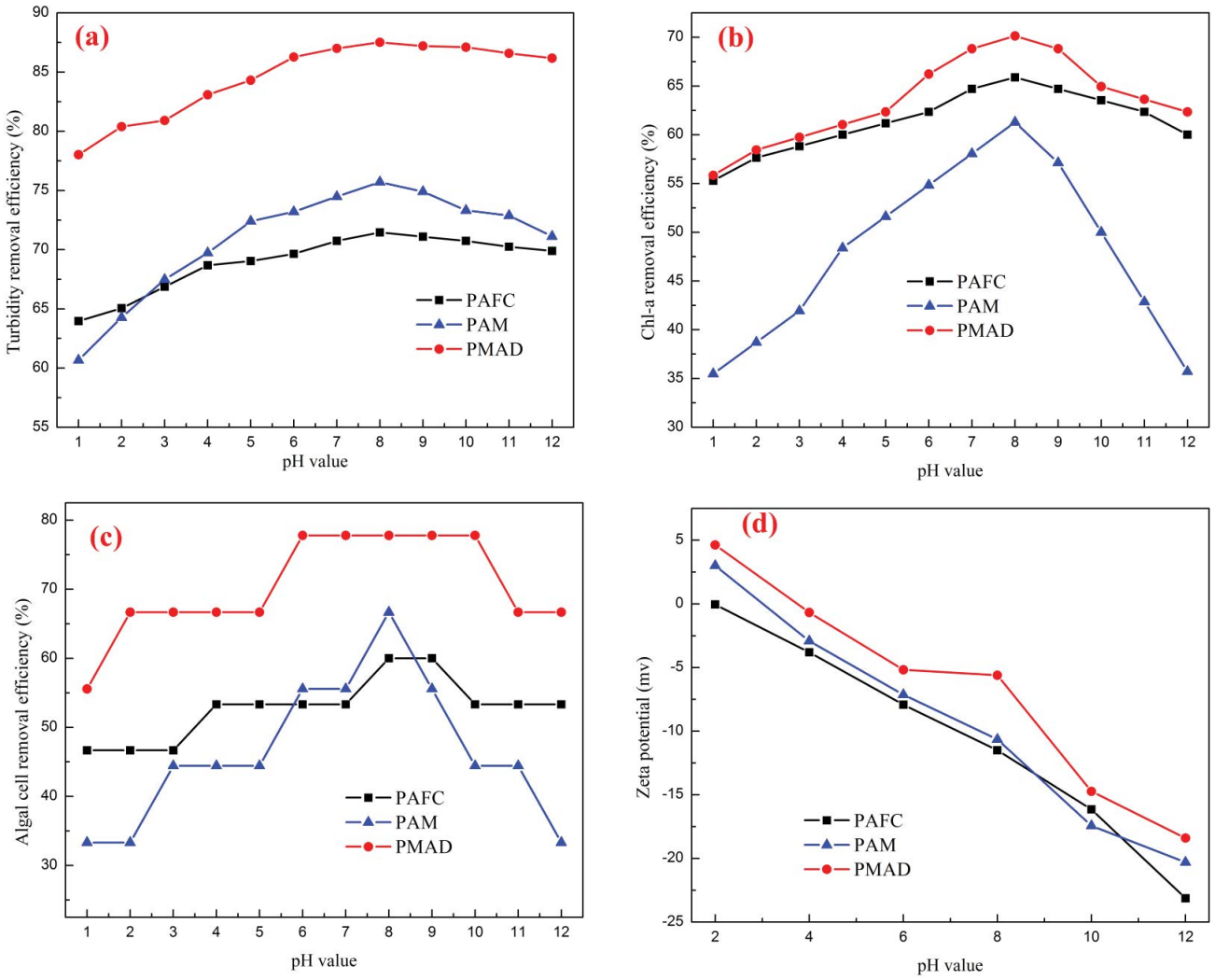

Fig. 13. Effects of pH on flocculation efficiency: (a) effects of pH on turbidity removal efficiency, (b) effects of pH on chl-a removal efficiency, (c) effects of pH on algal cell removal efficiency and (d) effects of pH on zeta potential. (PMAD dosage: 6 mg L^{-1}, PAM dosage: 6 mg L^{-1}, PAFC dosage: 40 mg L^{-1}, 350 r min^{-1} for 3 min, 70 r min^{-1} for 15 min, sedimentation: 15 min, temperature: 25°C).

Fig. 13d, the surface of the particles in the aqueous solution is positively charged when the pH was 2. Its zeta potential decreases with pH content.

The experiments results showed that the flocculation works better at weak acid and weak alkaline conditions. When the pH is equal, the flocculation performance of PMAD on algae-containing wastewater is significantly better than that of PAM and PAFC. This is because of the concentration of H^+ and OH^- in the solution changes with pH, which affects the changeability of the colloidal particles. Thus it affects the electrical neutralization between the flocculants and the particles. The zeta potential is greater than 0 under acidic conditions. And the positive charges on the molecular chain repel each other, which is not conducive to the continuous increase of flocs. PMAD undergoes a certain degree of degradation under acidic conditions due to the hydrolysis of chitosan, which further leads to a poor flocculation effect under acidic conditions. The colloidal particles in the solution are negatively charged with OH^-. Under the work of electrical neutralization, the colloidal particles are adsorbed by the positively charged flocculant. So the repulsive force between the colloidal particles is weakened [44]. And the flocculation of the bridging bridge is more likely to occur. The colloidal particles aggregate into a mass to form flocs, which eventually precipitate. When the pH is too high, the hydrogen ions generated by the hydrolysis of the flocculant are neutralized by the OH^-. So the flocculation performance is not exerted, resulting in deterioration of the flocculation effect.

3.3.3. Effects of G^{-1} on flocculation efficiency

As shown in Fig. 14, the removal rate of turbidity increased as G value increased and decreased after reaching the maximum value. The removal rate of turbidity by PMAD, PAM and PAFC at G value 500 s^{-1} was 94.9%, 91.9% and 80.9%,

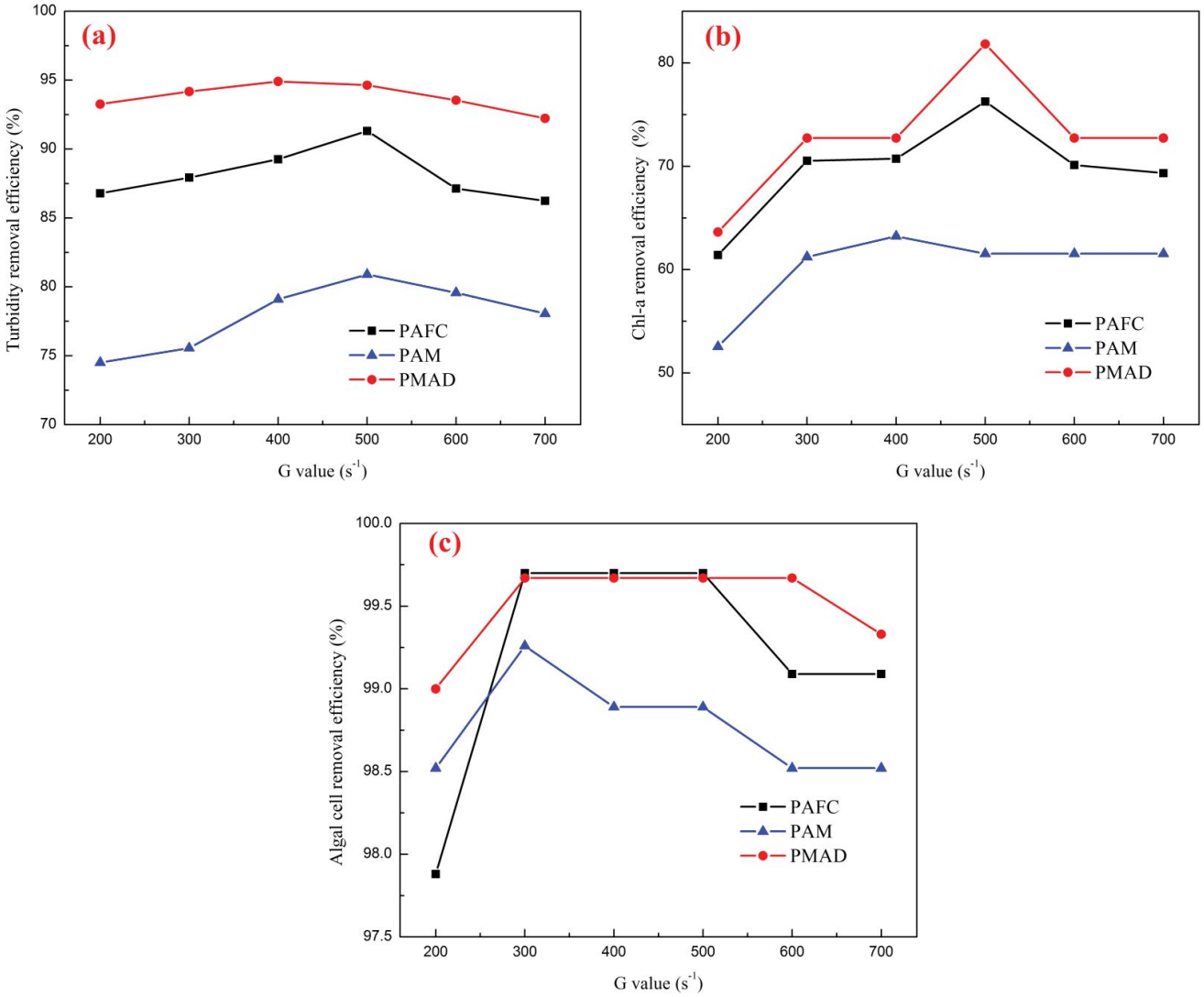

Fig. 14. Effects of G value on flocculation efficiency: (a) effects of G value on turbidity removal efficiency, (b) effects of G value on Chl-a removal efficiency and (c) effects of G value on algal cell removal efficiency. (PMAD dosage: 6 mg L^{-1}, PAM dosage: 6 mg L^{-1}, PAFC dosage: 40 mg L^{-1}, pH: 8, 350 r min^{-1} for 3 min, 70 r min^{-1} for 15 min, sedimentation: 15 min, temperature: 25°C).

respectively. The removal rate of algae cell concentration increases with *G* value, and decrease after reaching the maximum value. When the removal effect of algae cell concentration is optimum. At this time, the removal rate of algae cell concentration by PMAD, PAM, and PAFC at *G* value 300 s^{-1} was 99.7%, 98.9% and 99.6%, respectively. The removal rate of Chl-a increases with the increase of *G* value decreases slowly after reaching the maximum value. When *G* is 500 s^{-1}, the removal rate of Chl-a by PMAD and PAFC were 81.2% and 75%, respectively. When G is 400 s^{-1}, the removal efficiency of Chl-a by PAM was 69.2%. In addition, the flocculation effect of PMAD is slightly better than that of PAFC, which is obviously better than that of PAM at the same *G* value.

These results may cause by the following reasons. The first is that the colloid in the sample water cannot fully contact with the flocculant with low stirring speed. This leads to the situation that the flocculant is not easy to form. Besides, the pressure in the fluid is small, so the structure of the airbag cannot be damaged easily [45]. Furthermore, the structure of the airbag adjusted to re-suspend the algae after the algae settle. So the flocculation performance is weakened. As the stirring speed increases, the flocculant collides with the colloidal substance. The long-chain structure of the flocculant exerts the adsorption bridge effect so that the tiny particles in the water aggregate into large flocs and then settle. When the stirring speed is too fast, the rapid rotation of the stirring paddle will cause the flocs generated during flocculation to be broken, which affects the sedimentation of the flocs. And the adsorption bridging during the flocculation process produces a larger floc with a large specific surface area [46]. And some flocs are easily resuspended, resulting in a relatively low removal rate of turbidity, Chl-a and algae cell concentration.

4. Conclusion

In this study, a high-molecular flocculant PMAD was synthesized by using the UVS-initiated method with MCS, AM, and DMDAAC as monomers. The optimal synthesis conditions were explored. The contents of the experiment included monomer concentration, MCS concentration, monomer ratio, Initiation time, photoinitiator concentration. The experimental results showed that the optimal synthesis condition were that: the monomer concentration 12.5%, the percentage of maleated chitosan 10%, mMSC:mAM:mDMDAAC = 1:5:4, the photoinitiator concentration 0.3%, and the illumination time 120 min. Percentage yield of the final product PMAD is 90%–95%. SEM characterization indicated that PMAD has a porous, layered structure. The algae-containing wastewater was treated with the polymer synthesized under these conditions, and the optimal flocculation conditions were investigated. The removal rates of turbidity, Chl-a and COD were measured under different dosages, *G* values and pH conditions. The experimental results showed that When the PMAD dosage was 6 mg L^{-1}, the pH was 8, and the *G* value was 400, the coagulation effect is the best. At this time, the removal rate of turbidity, OD 680, Chl-a by PAMD at dosage 6 mg L^{-1}, pH 8, and G value 400 s^{-1} was 94.9%, 99.7% and 81.2%, respectively. Through the study of zeta potential, it was found that the flocculation mechanism of PMAD was mainly the function of the adsorption bridge and charge neutralization. The synthetic flocculant has better flocculation capacity on algae-containing wastewater than the commercially available flocculant and has good prospects for removal of algae-containing wastewater.

Acknowledgments

This research was supported by National Natural Science Foundation of China (No. 51508268), National Key Research and Development Program of China (2017YFB0602500), and 2018 Six Talent Peaks Project of Jiangsu Province (JNHB-038).

References

[1] B. Ghernaout, D. Ghernaout, A. Saiba, Algae and cyanotoxins removal by coagulation/flocculation: a review, Desal Wat. Treat, 20 (2010) 133–143.
[2] Y. Gerchman, B. Vasker, M. Tavasi, Y. Mishael, Y. Kinel-Tahan, Y. Yehoshua, Effective harvesting of microalgae: comparison of different polymeric flocculants, Bioresour. Technol., 228 (2017) 141–146.
[3] S.B. Ummalyma, E. Gnansounou, R.K. Sukumaran, R. Sindhu, A. Pandey, D. Sahoo, Bioflocculation: an alternative strategy for harvesting of microalgae – an overview, Bioresour. Technol., 242 (2017) 227–235.
[4] S.A. Fast, V.G. Gude, Ultrasound-chitosan enhanced flocculation of low algal turbid waters, J. Ind. Eng. Chem., 24 (2015) 153–160.
[5] D. Zeng, J. Wu, J.F. Kennedy, Application of a chitosan flocculant to water treatment, Carbohydr. Polym., 71 (2007) 135–139.
[6] S. Woranuch, R. Yoksan, Preparation, characterization and antioxidant property of water-soluble ferulic acid grafted chitosan, Carbohydr. Polym., 96 (2013) 495–502.
[7] B. Wang, Y. Zhang, C.B. MIAO, Preparation of cationic chitosan-polyacrylamide flocculant and its properties in wastewater treatment, J. Ocean Univ. China, 10 (2011) 42–46.
[8] C. Dong, W. Chen, C. Liu, Flocculation of algal cells by amphoteric chitosan-based flocculant, Bioresour. Technol., 170 (2014) 239–247.
[9] F.A. Al Sagheer, K.D. Khalil, E.I. Ibrahim, Synthesis and characterization of chitosan-g-poly(2-(furan-2-carbonyl)-acrylonitrile): grafting of chitosan using a novel monomer prepared by a Baylis–Hillman reaction, Eur. Polym. J., 49 (2013) 1662–1672.
[10] T. Lü, S. Zhang, D. Qi, D. Zhang, H. Zhao, Enhanced demulsification from aqueous media by using magnetic chitosan-based flocculant, J. Colloid Interface Sci., 518 (2018) 76–83.
[11] G. Ma, D. Yang, J.F. Kennedy, J. Nie, Synthesize and characterization of organic-soluble acylated chitosan, Carbohydr. Polym., 75 (2008) 390–394.
[12] B.B. Zhang, J. Bai, G.J. Yuan, Y.Y. Jia, Z.X. Han, Z.G. Zhao, M.Y. Miao, H.Q. Su, Ecofriendly flocculation of bentonite suspensions by two anionic polysaccharides: carboxylated chitosan (CC) and sodium carboxymethyl starch (CMS-Na), Adv. Mater. Res., 955–959 (2014) 321–325.
[13] S. Ding, X. Zhang, X. Feng, Y. Wang, S. Ma, Q. Peng, W. Zhang, Synthesis of N, N′-diallyl dibenzo 18-crown-6 crown ether crosslinked chitosan and their adsorption properties for metal ions, React. Funct. Polym., 66 (2005) 357–363.
[14] M. Dharani, S. Balasubramanian, Synthesis, characterization and application of acryloyl chitosan anchored copolymer towards algae flocculation, Carbohydr. Polym., 152 (2016) 459–467.
[15] E.S. Beach, M.J. Eckelman, Z. Cui, L. Brentner, J.B. Zimmerman, Preferential technological and life cycle environmental performance of chitosan flocculation for harvesting of the green algae Neochloris oleoabundans, Bioresour. Technol., 121 (2012) 445–449.
[16] L. Chen, Y. Sun, W. Sun, K.J. Shah, Y. Xu, H. Zheng, Efficient cationic flocculant MHCS-g-P(AM-DAC) synthesized by UV-induced polymerization for algae removal, Sep. Purif. Technol., 210 (2019) 10–19.

[17] J. Wang, Y. Chen, S. Zhang, H. Yu, A chitosan-based flocculant prepared with gamma-irradiation-induced grafting, Bioresour. Technol., 99 (2007) 3397–3402.
[18] Standard for Water Conservancy Industry of China, Water Quality - Determination of Chlorophyll by Spectrophotometry (SL 88-2012), Ministry of Water Resources of China, China, 2012.
[19] China National Standard, Chemicals – Alga Growth Inhibition Test (GB/T 21805-2008), The State Bureau of Quality and Technical Supervision and China National Standardization Management Committee, 2008.
[20] China National Standard, Colloidal System – Methods for Zeta Potential Determination – Part 1: Electroacoustic and Electro Kinetic Phenomena (GB/T 32671.1-2016), The State Bureau of Quality and Technical Supervision and China National Standardization Management Committee, 2016.
[21] Z. Yang, H. Yang, Z. Jiang, T. Cai, H. Li, H. Li, A. Li, R. Cheng, Flocculation of both anionic and cationic dyes in aqueous solutions by the amphoteric grafting flocculant carboxymethyl chitosan- graft -polyacrylamide, J. Hazard. Mater., 254–255 (2013) 36–45.
[22] D. Wang, T. Zhao, L. Yan, Z. Mi, Q. Gu, Y. Zhang, Synthesis, characterization and evaluation of dewatering properties of chitosan-grafting DMDAAC flocculants, Int. J. Biol. Macromol., 92 (2016) 761–768.
[23] B. Liu, H. Zheng, Y. Wang, X. Chen, C. Zhao, Y. An, X. Tang, A novel carboxyl-rich chitosan-based polymer and its application for clay flocculation and cationic dye removal, Sci. Total Environ., 640–641 (2018) 107–115.
[24] O. Molatlhegi, L. Alagha, Adsorption characteristics of chitosan grafted copolymer on kaolin, Appl. Clay Sci., 150 (2017) 342–353.
[25] C. Zhong, J. Wu, C.A. Reinhart-King, C.C. Chu, Synthesis, characterization and cytotoxicity of photo-crosslinked maleic chitosan–polyethylene glycol diacrylate hybrid hydrogels, Acta Biomater, 6 (2010) 3908–3918.
[26] Y. Zhenzhen, D. Qifeng, L. Chengsheng, C. Dongsu, Z. Haifeng, Z. Wenjing, Z. Qianqian, F. Bing, Preparation and characterization of poly(maleic acid)-grafted cross-linked chitosan microspheres for Cd(II) adsorption, Carbohydr. Polym., 172 (2017) 28–39.
[27] H. Zheng, Y. Sun, J. Guo, F. Li, W. Fan, Y. Liao, Q. Guan, Characterization and evaluation of dewatering properties of PADB, a highly efficient cationic flocculant, Ind. Eng. Chem. Res., 53 (2014) 2572–2582.
[28] A. Srivastava, D.K. Mishra, K. Behari, Graft copolymerization of -vinyl-2-pyrrolidone onto chitosan: synthesis, characterization and study of physicochemical properties, Carbohydr. Polym., 80 (2010) 790–798.
[29] Y. Liao, H. Zheng, Q. Li, Y. Sun, D. Li, W. Xue, UV-initiated polymerization of hydrophobically associating cationic polyacrylamide modified by a surface-active monomer: a comparative study of synthesis, characterization, and sludge dewatering performance, Ind. Eng. Chem. Res., 53 (2014) 11193–11203.
[30] Y. Sun, C. Zhu, W. Sun, Y. Xu, X. Xiao, H. Zheng, H. Wu, C. Liu, Plasma-initiated polymerization of chitosan-based CS-g-P(AM-DMDAAC) flocculant for the enhanced flocculation of low-algal-turbidity water, Carbohydr. Polym., 164 (2017) 222–232.
[31] X. Li, H. Zheng, B. Gao, Y. Sun, B. Liu, C. Zhao, UV-initiated template copolymerization of AM and MAPTAC: microblock structure, copolymerization mechanism, and flocculation performance, Chemosphere, 167 (2017) 71–81.
[32] X. Zhang, G. Jiang, Y. Xuan, L. Wang, X. Huang, Associating copolymer acrylamide/diallyldimethylammonium chloride/butyl acrylate/2-acrylamido-2-methylpropanesulfonic acid as a tackifier in clay-free and water-based drilling fluids, Energy Fuels, 31 (2017) 4655–4662.
[33] Y. Liao, X. Zheng, Z. Zhang, B. Xu, Y. Sun, Y. Liu, H. Zheng, Ultrasound-assisted polymerization of P(AM-DMDAAC): synthesis, characterization and sludge dewatering performance, J. Environ. Chem. Eng., 5 (2017) 5439–5447.
[34] J. Zhu, H. Zheng, Z. Jiang, Z. Zhang, L. Liu, Y. Sun, T. Tshukudu, Synthesis and characterization of a dewatering reagent: cationic polyacrylamide (P(AM–DMC–DAC)) for activated sludge dewatering treatment, Desal. Wat. Treat., 51 (2013) 2791–2801.
[35] L. Feng, S. Liu, H. Zheng, J. Liang, Y. Sun, S. Zhang, X. Chen, Using ultrasonic (US)-initiated template copolymerization for preparation of an enhanced cationic polyacrylamide (CPAM) and its application in sludge dewatering., Ultrason. Sonochem., 44 (2018) 53–63.
[36] X. Li, H. Zheng, Y. Wang, Y. Sun, B. Xu, C. Zhao, Fabricating an enhanced sterilization chitosan-based flocculants: synthesis, characterization, evaluation of sterilization and flocculation, Chem. Eng. J., 319 (2017) 119–130.
[37] Z. Abdollahi, M. Frounchi, S. Dadbin, Synthesis, characterization and comparison of PAM, cationic PDMC and P(AM-DMC) based on solution polymerization, J. Ind. Eng. Chem., 17 (2011) 580–586.
[38] B. Riaño, B. Molinuevo, M.C. García-González, Optimization of chitosan flocculation for microalgal-bacterial biomass harvesting via response surface methodology, Ecol. Eng., 38 (2011) 110–113.
[39] A. Bhattacharya, A. Malik, H.K. Malik, A mathematical model to describe the fungal assisted algal flocculation process, Bioresour. Technol., 244 (2017) 975.
[40] L. Lv, X. Zhang, J. Qiao, Flocculation of low algae concentration water using polydiallyldimethylammonium chloride coupled with polysilicate aluminum ferrite, Environ. Technol., 39 (2017) 1–8.
[41] K. He, T. Lou, X. Wang, W. Zhao, Preparation of lignosulfonate–acrylamide–chitosan ternary graft copolymer and its flocculation performance, Int. J. Biol. Macromol., 81 (2015) 1053–1058.
[42] S. Haufe, J. Bohrisch, D. Schwarz, S.Y. Bratskaya, C. Steinbach, S. Schwarz, Flocculation efficiency of reacetylated water soluble chitosan versus commercial chitosan, Colloids Surf., A, 532 (2017) 222–227.
[43] G. Conzatti, S. Chamary, N. De Geyter, S. Cavalie, R. Morent, A. Tourrette, Surface functionalization of plasticized chitosan films through PNIPAM grafting via UV and plasma graft polymerization, Eur. Polym. J., 105 (2018) 434–441.
[44] F. Roselet, D. Vandamme, M. Roselet, K. Muylaert, P.C. Abreu, Effects of pH, Salinity, biomass concentration, and algal organic matter on flocculant efficiency of synthetic versus natural polymers for harvesting microalgae biomass, Bioenergy Res., 10 (2017) 1–11.
[45] H. Pei, C. Ma, W. Hu, F. Sun, The behaviors of Microcystis aeruginosa cells and extracellular microcystins during chitosan flocculation and flocs storage processes, Bioresour. Technol., 151 (2014) 314–322.
[46] T.L. Gp, M.H. Vermuë, G. Olivieri, V.D.B. La, M.J. Barbosa, M.H. Eppink, R.H. Wijffels, D.M. Kleinegris, Cationic polymers for successful flocculation of marine microalgae, Bioresour. Technol., 169 (2014) 804–807.